Center for Advanced Multimodal Mobility Solutions and Education

Project ID: 2017 Project 04

CORRIDOR LEVEL ADAPTIVE SIGNAL CONTROL

Interim Report

by

Hao Liu, M.S. (ORCID ID: https://orcid.org/0000-0002-5319-9514)
The University of Texas at Austin

and

Randy Machemehl, Ph.D., P.E. (ORCID ID: https://orcid.org/0000-0002-4045-2023)
Professor, Department of Civil and Environmental Engineering
The University of Texas at Austin
301 E. Dean Keeton Street, Stop C1761, Austin, TX 78712
Phone: 1-512-471-4541; Email: rbm@mail.utexas.edu

for

Center for Advanced Multimodal Mobility Solutions and Education
(CAMMSE @ UNC Charlotte)
The University of North Carolina at Charlotte
9201 University City Blvd
Charlotte, NC 28223

September 2018

ACKNOWLEDGMENTS

This project was funded by the Center for Advanced Multimodal Mobility Solutions and Education (CAMMSE @ UNC Charlotte), one of the Tier I University Transportation Centers that were selected in this nationwide competition, by the Office of the Assistant Secretary for Research and Technology (OST-R), U.S. Department of Transportation (US DOT), under the FAST Act. The authors are also very grateful for all of the time and effort spent by DOT and industry professionals to provide project information that was critical for the successful completion of this study.

DISCLAIMER

Table of Contents

List of Figures

List of Tables

EXECUTIVE SUMMARY

With the increasing number of vehicles, most cities around the world are suffering from traffic congestion. A variety of strategies can be employed to address the congestion problem, such as traffic signal control, constructing new roads, allocating dedicated lanes for public transit, and road space rationing. Out of these solutions, traffic signal control is the most cost-effective way to mitigate congestion since its objective is to maximize the traffic mobility by allocating the green time to each signal phase in the most reasonable way without monetary cost on the construction of infrastructure.

Signal control can be classified into two groups: pre-timed signal control and adaptive signal control. In the pre-timed control method, signal timings are established based on historical data and implemented to the specific time of day. Unlike the pre-timed control, adaptive signal control optimizes signal timing plans based on real-time traffic conditions. Thanks to its ability to adjust and respond to the prevailing traffic condition, adaptive control is superior to pre-timed control. Although adaptive signal control offers promise in reducing traffic congestion, it is not very popular in urban networks because of its complexity. For instance, the City of Austin manages about 1,020 traffic signals and almost all of them are pre-timed. Therefore, the adaptive signal control is still a challenging and necessary research topic.

The core elements of an adaptive signal control method include a traffic volume prediction model and a signal optimization model. The main considerations of the adaptive control method are prediction accuracy and computational speed. In most published adaptive signal control methods, upstream traffic detectors are frequently used for traffic prediction. Given the short distance between the sensors and the target intersection, this method cannot provide enough information for the projection horizon. Therefore, approximations are made based on the historical information and the correlation in time. Although these models may work well under traffic conditions with low variation, model efficiency cannot be assured when traffic volumes change dramatically. Moreover, the traffic flow model used in the optimization part is usually approximated. For example, to have a deterministic expression for the control delay during the red time, some models assume a Poisson process for the arriving vehicles and constant arrival rates in each iteration, which may not be appropriate in reality.

This study proposes an adaptive signal control algorithm to optimize the signal timing for the incoming cycle at an isolated intersection. A CTM-based model predicts the traffic volumes for the target intersection by counting the current vehicle numbers in the upstream cells. This model does not make assumptions about the arrival process and the correlation of the flows between consecutive cycles. Through this method, the accuracy of the volume prediction is ensured even under rapidly varying traffic conditions. In addition, the signal optimization problem is modeled as a mixed integer linear program (MILP) based on the Barron-Jensen/Frankowska (B-J/F) solution to the Lighthill-Whitham-Richards (LWR) model. The sequence and the splits of phases can be optimized at the same time according to the current traffic condition. Finally, this study compares the new method to the critical lane flow ratio method, which is a commonly used strategy. It shows that the proposed method can reduce the traffic delay under various traffic congestion degrees for both balanced and unbalanced traffic volumes. The delay reduction percentage increases with decreases of the overall critical volume-to-capacity ratio. The reduction is

statistically significant when the overall critical volume-to-capacity ratio is below 0.9, and it can reach 32% when the overall critical volume-to-capacity ratio is equal to 0.347 under unbalanced traffic conditions.

Chapter 1. Introduction

1.1 Problem Statement

With increases in car ownership, congestion has become a worldwide problem in urban traffic networks, especially in large cities. Various methods can be employed to mitigate the congestion, such as dedicated lanes, road pricing, and access restriction. Compared to these methods, traffic signal control is a more cost-effective solution to improve the efficiency of the traffic network, and it has drawn much research attention in the past decades.

In general, traffic signal control techniques can be divided into two groups based on the control mechanism: pre-timed control and adaptive control. In pre-timed control, different signal parameters, including cycle length, phase splits, and phase sequences, are designed from historical data and implemented at predetermined periods of a day. This method is not efficient if the traffic condition varies significantly from day to day. On the other hand, the goal of adaptive control is to provide the optimal signal timing for the prevailing traffic condition. Adaptive signal timing changes according to the traffic volume prediction to optimize specific measures of effectiveness such as travel delay, stop delay, and throughput rate. It is considered superior to pre-timed control thanks to its ability to adjust to varying traffic demands in time.

For a signalized intersection, traffic flow prediction and traffic signal optimization are two kernel components of the adaptive control method. Generally, traffic flow prediction is achieved by combing current state measurements from sensors and approximation models. After that, optimal signal timings are obtained based on the optimization model and the traffic volume prediction. A favorable adaptive control method needs to possess two qualities: high prediction accuracy and fast computation speed. The first quality ensures the optimal signal timings match the real upcoming traffic volume; the second quality is necessary to change the signal timing plans in time.

1.2 Objectives

The objective of this study is to (1) develop a traffic volume prediction model that can be used under rapidly varying traffic conditions; (2) propose a traffic optimization model based on the analytical solution of the LWR model; (3) prove the effectiveness of the proposed model through microscopic traffic simulations.

1.3 Expected Contributions

To accomplish these objectives, several tasks have been undertaken. First, a movement-based CTM model is proposed to predict the traffic volume for the target intersection. By using this model, the traffic prediction is completely based on the traffic states of the upstream links so that this method can be applied to the rapidly varying traffic conditions. Second, after obtaining the traffic volume prediction, a mixed integer linear program (MILP) derived from the analytical solution of the Lighthill-Whitham-Richards (LWR) model is developed to optimize the traffic signal. Third, microscopic traffic simulations are executed by combing

CORSIM and Matlab to demonstrate the effectiveness of the proposed framework. It shows that compared to a traditional traffic signal design method, the critical lane flow ratio method, the proposed model can reduce traffic delay significantly.

1.4 Report Overview

The remainder of this report is organized as follows: Chapter 2 presents a comprehensive review of the adaptive signal control methods. Chapter 3 provides a detailed formulation for the proposed adaptive signal control framework. This chapter consists of three main parts: 1) A traffic volume prediction model is derived for an isolated intersection; 2) A traffic signal optimization model based on the LWR model is proposed; 3) Microscopic traffic simulations are executed by utilizing both CORSIM and Matlab to demonstrate the effectiveness of the proposed model. Chapter 4 summarizes the tasks completed in this study and discusses directions for future research.

Chapter 2. Literature Review

2.1 Introduction

This chapter provides a comprehensive review of the literature on various adaptive signal control methods.

2.2 Existing Adaptive Signal Control Methods

A large number of adaptive signal control methods have been proposed in the past decades. Two widely used traffic control strategies, SCOOT [1] and SCATS [2], choose the best signal timing plan according to the prevailing traffic condition, however, the efficiency of these systems is reduced with congested or rapidly varying traffic conditions.

To make an even more flexible adaptive signal control algorithm, Miller [3] proposed a dynamically self-optimizing strategy in which the decision of whether a phase should be extended is made periodically within a short interval. Although Bang and Nilsson [4] proved the advantages of Miller's method by comparing results from a fixed-time approach in a field test setting, the overall optimality of this method is not ensured because of the short projection horizon.

OPAC [5] and RHODES [6]–[8] use online data from upstream detectors and dynamic programming (DP) to find an optimal solution. The longest prediction horizon is equal to the distance between the intersection and the upstream detectors divided by the free flow speed. Because this distance is commonly not long enough for a long-interval prediction, these techniques resort to the rolling horizon scheme to address this issue.

Rolling Horizon Scheme

The rolling horizon scheme splits a project horizon into a "head" and a "tail". The traffic volumes in the "head" are obtained from detector measurements while the "tail" is approximated by models. Then, the optimal signal for the project horizon is computed, but only implemented for the "head" part. The process repeats itself at the end of the "head" part. The project horizon length has a critical impact on the performance: a short project horizon may lead to a shortsighted result; it is difficult to ensure high accuracy for a long project horizon. A more detailed comparison between different adaptive signal control methods can be found in [9].

Adaptive signal control requires the models be solved quickly enough so that the optimal signal timing can be implemented in time. Although the theoretically-sound models have high accuracy, the exponential increase in complexity limits their solving speed. Cai et al. [9] proposed an approximate dynamic programming approach to reduce the computational complexity to a polynomial to improve the computational speed of the algorithm and increase the signal revision frequency to enhance the model efficiency. The revision frequency is the frequency with which the model makes the decision to adjust signal timing settings. More

recently, Zheng and Recker [10], [11] proposed a control algorithm with a modified rolling horizon scheme to improve the computational speed. In their framework, arrivals are assumed to be a Poisson process with constant arrival rate in each iteration that is predicted based on the traffic volume of the previous horizon and an approximation model. Due to this Poisson arrival assumption, the performance of the control systems deteriorates under congested traffic conditions.

Although the rolling horizon is widely used in adaptive signal control methods, Newell [12] proposed a control policy in which the traffic signal should shift to serve another phase when the queue of the current phase is dissipated, and he proved that the rolling horizon scheme might cause more traffic delay under some situations. This proposed policy is called exhaustive service discipline in polling systems. Mirchandani and Zou [13] developed a queueing model to analyze the parameters, such as cycle length, split length and average delay for this policy. Besides the model used for an isolated intersection working under uncongested traffic conditions, Aboudolas et al. [14] developed a quadratic-programming model to balance the queue lengths under congested traffic conditions at the network level.

In addition to accurate traffic volume prediction, the optimization model formation is crucial to adaptive signal control. A wide variety of measures of effectiveness are used to inform adaptive signal optimization models, such as control delay, total delay, queue length, stop times, person delay, and total throughput. Assuming the average vehicle occupancies of different vehicle types are given, Christofa et al. [15] proposed a model to minimize person delay on the arterial streets with platoons. The traffic flow models in most of the systems mentioned in the previous paragraph are approximated to make it efficient to solve. For example, besides the problem of forecasting interval length, RHODES [6]–[8] does not consider the queue length at the target intersection when it computes the travel time between two detectors; in Zheng and Recker's model [10], [11], although they assumed arrivals to be a Poisson process (stochastic process), the arrival and departure processes in their model have constant rates because they can only model averages and do not consider variability. Although detectors are commonly used to provide data for traffic volume prediction, they may not be installed at some intersections, and in this case, only the historical data might be available for designing signal timings. Because of the random nature of the traffic arrivals, Lo [16] developed an approach to analyze the phase clearance reliability (PCR) of traffic signals to obtain the probabilistic evolution of overflow from one cycle to the next cycle, assuming the distribution of the arrival rate is given. Based on this method, Lubing Li et al. [17] and Wanjing Ma et al. [18] developed coordinated adaptive signal control methods as a multi-stage program to minimize the expected delay along the arterial with coordinated signal timing.

2.3 Summary

A comprehensive review of past research of on the adaptive signal control problem has been discussed in the preceding section.

Chapter 3. Solution Methodology

3.1 Introduction

In this section, we propose an adaptive signal control algorithm for an isolated intersection in a surveillance environment. In our framework, the traffic signal is updated every cycle. At the beginning of each cycle, the traffic densities on the upstream links are obtained from the surveillance system. Then, a movement-based cell transmission model (CTM) [19], [20] is used to forecast the traffic volumes for the next cycle. Using this method, the model does not make assumptions about the incoming traffic volumes, such as vehicle arrival rates and their correlation to previous cycles. In addition, this study presents an optimization model from the analytical solution [21]–[23] of the Lighthill-Whitham-Richards (LWR) [24] model. The optimal signal timing plan comes from combining the predicted traffic volumes and this optimization model. The lost time, cycle time, and minimum green time are preset, other parameters such as the phase sequence, phase splits, and the number of switchovers are optimized in our framework. CORSIM is a popular microscopic traffic simulator that has the ability to simulate the complex elements in the traffic system, such as driving behavior, vehicle types and road configuration. CORSIM applies the optimal signal plans to microscopic simulations to investigate the performance of the proposed framework. The optimal signal timings are solved with a mathematical programming solver, CPLEX, embedded in MATLAB.

3.2 Overview of the Proposed Method

The time horizon for this method is the predetermined cycle length. The time space is divided into time steps and the traffic lanes are divided into spatial segments. The overall steps of this method are as follows:

- At the beginning of a signal cycle, the number of vehicles in every segment in the network is obtained by the surveillance system.
- First, the initial densities of the links connecting the target intersection are computed for the optimization model.
- Second, by inserting the upstream vehicle number information into a CTM-based model, we obtain the predicted traffic volumes approaching the target intersection during this cycle.
- Next, a proposed signal optimization model and the predicted traffic volume are used to obtain and assign the optimal traffic signal timing in this cycle.

These steps are repeated at the beginning of each cycle.

3.3 Traffic Prediction Model

In this study, a commonly used signal phase configuration shown in Figure 3-1 is adopted to demonstrate the algorithm. This configuration is composed of 8 movements (numbered in Figure 3-1) and 4 phases, and the movements in the same column are served by the same phase. Phase 1 includes the movements in the first column, Phase 2 includes the movements in the second column, so on and so forth. The following assumptions are made:

1. The movements in each phase are fixed, which means every pair of movements (1+2, 3+4, 5+6 and 7+9) always start and end at the same time;
2. The all red time is the lost time. Yellow time and start-up delay are not considered;
3. Each phase has a separate lane, meaning vehicles do not have to yield to each other. In CTM, we divide the lanes into cells based on their channelization to obtain the densities for each movement. For example, if a link has one lane for left turns and another lane for through and right-turn movements, we divide each lane into cells and assume all the vehicles in the left cells are turning left and all the vehicles in the right cells are going through or turning right;
4. All of the signal timings excluding the one at the target intersection are known; and
5. The turning movement percentages are known.

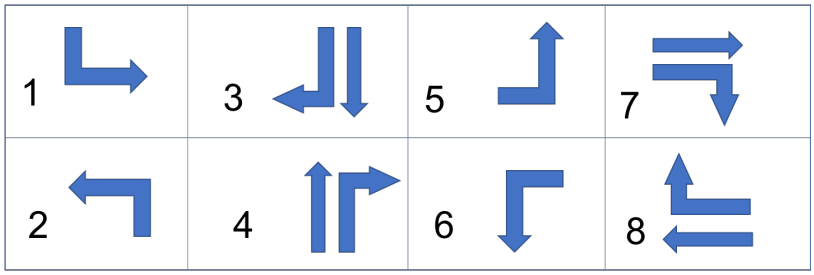

Figure 3-1 A commonly used traffic signal design.

The notation used in this section are defined as follows:

X: cell length (feet);
T: time step size (s);
N : set of time steps;
C: cycle length (s);
V: upstream node index;
v_f: free flow speed (mph);
w : congestion speed (mph);
i: index of movements;
I: number of the movements;
r : index of phases;
R : set of phases;
h: index of cells;
n_h: number of cells;
c_{Vi}: saturation flow of movement *i* at intersection *V;*
$q_i(t)$: prediction of the volume for movement *i* at time *t* (vph);
$\delta_{V_i}(t)$: 0, if the phase serving movement *i* is red at time *t* at node *V;* 1, otherwise.
$S_{V_i}(t,k)$: sending flow of the kth cell of movement *i* at time t at intersection *V;*
$R_{V_i}(t,k)$: receiving flow of the kth cell of movement *i* at time t at intersection *V;*
$n_{V_i}(t,k)$: number of vehicles in the kth cell of movement *i* at time t at intersection *V;*

In this study, we assume that the relationship between the flow and the density of each movement follows the triangular fundamental diagram, and the calibration of the model parameters will be described in the case study section of this report. At time t (the beginning of a cycle at the target intersection), the vehicle number in each cell is measured by the surveillance system. Then, the CTM model predicts the traffic inflow for each movement (shown in Figure 1) at the target intersection. The prediction scenario geometry is shown in Figure 3-2.

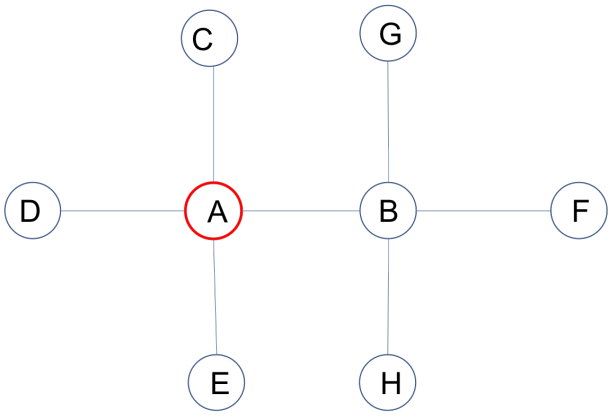

Figure 3-2 Prediction scenario geometry.

In Figure 3-2, node A is the target intersection, the incoming volumes for links BA, EA, DA, and CA in this cycle are required to perform the signal optimization. The traffic volume for link BA is predicted from the upstream links FB, HB, and GB through the following method, and other inflows can be completed using the same manner. From the CTM model, at iteration t, the sending flow of each cell at intersection B is,

$$S_{B_i}(t,h) = \min\left(\frac{n_{B_i}(t,h) v_f T}{X}, c_{B_i} T \right), \quad \forall i \in [1, I], h \in [1, n_h], \tag{1}$$

the receiving flow is expressed as,

$$R_{B_i}(t,h) = \min\left(-w\left(\rho_m - \frac{n_{B_i}(t,h)}{X} \right) T, c_{B_i} T \right), \forall i \in [1,I], h \in [1, n_h], \tag{2}$$

and the number of vehicles in each cell at iteration t+1 is,

$$\begin{aligned} n_{B_i}(t+1,h) = n_{B_i}(t,h) &+ \min\left(R_{B_i}(t,h), S_{B_i}(t,h-1) \right) \\ &- \min\left(R_{B_i}(t,h+1), S_{B_i}(t,h) \right), \forall i \in [1, I], h \in [2, n_h - 1] \end{aligned}, \tag{3}$$

$$n_{B_i}(t+1,1) = n_{B_i}(t,1) - \min(R_{B_i}(t,2), S_{B_i}(t,1)), \tag{4}$$

$$n_{B_i}(t+1,n_h) = n_{B_i}(t,n_h) + \min(S_{B_i}(t,n_h - 1), R_{B_i}(t,n_h)) - \min(S_{B_i}(t,n_h), c_{B_i} \delta_{B_i}(t) T). \tag{5}$$

In this method, we assume the upstream links FB, GB, and HB are longer than Cv_f, and the entry flows to these links = 0 because the entering vehicles cannot arrive at node B in one cycle even if they travel at the free flow speed. Therefore, the expression of the number of vehicles in the first cell of each movement at the next time step shown as (4) does not consider the inflow. Similarly, because our method works for a non-spillback situation, we assume the receiving flow of link BA is always equal to the capacity, and the outflow at node B is only constrained by the signal, as shown in (5). The traffic volumes for movements 6 and 8 shown in Figure 3-1 at node A come from link BA, and the predicted volumes are expressed as,

$$\begin{cases} q_6(t) = \left(\sum_{i \in [1, I]} \min(S_{B_i}(t, n_h), c_{B_i} \delta_{B_i}(t) T) \beta_i \right) \alpha_6 \\ q_8(t) = \left(\sum_{i \in [1, I]} \min(S_{B_i}(t, n_h), c_{B_i} \delta_{B_i}(t) T) \beta_i \right) \alpha_8 \end{cases}, \tag{6}$$

where β_i is the percentage of the vehicle number from movement *i* entering link BA, α_6 and α_8 are the corresponding turning movement percentage of link BA. The inflows of other movements in the coming cycle can be predicted using the same manner.

For simplicity, in the CTM model above we assume the upstream link length is only long enough to consider the incoming links at the intersections next to the target intersection (B, C, D, E in Figure 3-2) to predict the traffic inflow of each approach. If they are not long enough, we cannot assume zero inflows for these upstream links, and the inflows for the upstream nodes need to be predicted using equations (1) through (6).

3.4 Signal Optimization Model

In traffic flow theory, Lighthill-Whitham-Richards (LWR) model [25] is widely used to depict the evolution of traffic flow,

$$\frac{\partial \rho(t,x)}{\partial t} + \frac{\partial \psi(\rho(t,x))}{\partial x} = 0 , \tag{7}$$

where $\rho(t,x)$ is the density of at the point x away from a reference point in time t, and ψ is the Hamiltonian, which is used to denote the experimental relationship between flow and density. For simplicity, a triangular fundamental diagram is used to represent the relationship between flow and density such that,

$$\psi(\rho) = \begin{cases} v_f \rho, & \rho \in [0, \rho_c] \\ w(\rho - \rho_f), & \rho \in [\rho_c, \rho_m] \end{cases}, \tag{8}$$

where v_f is the free flow speed, w is the congestion speed, ρ_c is the critical density when flow is at its maximum, ρ_m is the jam density, where the flow is zero due to complete congestion.

Alternatively, traffic flow can be modeled using the Moskowitz function $M(t,x)$, representing a vehicle index at (t,x) [26]. Then Hamilton-Jacobi PDE (H-J PDE) can be obtained from the integration of the LWR model in space,

$$\frac{\partial M(t,x)}{\partial t} - \psi(-\frac{\partial M(t,x)}{\partial x}) = 0 . \tag{9}$$

To solve equation (9), a traffic link with a spatial domain $[\xi,\chi]$, where ξ is the upstream boundary and χ is the downstream boundary, is divided evenly into $k_{\max}$ segments; the time domain $[0,t_{\max}]$, where $t_{\max}$ is the simulation time, is divided evenly into $n_{\max}$ time steps. In addition, $K=\{1,...,k_{\max}\}$ and $N=\{1,...,N_{\max}\}$. The initial conditions of a traffic link are defined as

$$M_k(t,x)=\begin{cases} -\sum_{i=1}^{k-1}\rho(i)X \\ -\rho(k)(x-(k-1)X), & if\ t=0 \\ & and\ x\in[(k-1)X,kX] \\ +\infty, & otherwise \end{cases}, \tag{10}$$

the upstream boundary conditions are

$$\gamma_n(t,x)=\begin{cases} -\sum_{i=1}^{n-1}q_{in}(i)T \\ +q_{in}(n)(t-(n-1)T), & if\ x=\xi \\ & and\ t\in[(n-1)T,nT] \\ +\infty, & otherwise \end{cases}, \tag{11}$$

and the downstream boundary conditions are

$$\beta_n(t,x)=\begin{cases} -\sum_{i=1}^{n-1}q_{out}(i)T \\ +q_{out}(n)(t-(n-1)T) \\ -\sum_{k=1}^{k_{\max}}\rho(k)X, & if\ x=\chi \\ & and\ t\in[(n-1)T,nT] \\ +\infty, & otherwise \end{cases}, \tag{12}$$

where X and T are the length for the spatial segment and time segment, separately, $\rho(i)$ is the initial density for the *i*th spatial segment, $q_{in}(i)$ and $q_{out}(i)$ are the inflow and outflow, respectively, for the *i*th time segment at the upstream node and downstream nodes. We assume the density and flow in each initial and boundary segment are constants, so the Moskowitz functions (10)-(12) are piece-wise linear functions of time and space.

3.5 Analytical Solution to the HJ-PDE

The analytical solution to the H-J PDE (9) with initial and boundary conditions (10)-(12) are given by Claudel and Bayen [22]; Daganzo [27]. Below is a full description of the solution.

Definition 1 (Value Condition): A value condition $c(\cdot,\cdot)$ is a lower semicontinuous function defined on a subset of $[0,t_{\max}]\times[\xi,\chi]$.

In this problem, the initial conditions, upstream boundary conditions, and downstream boundary conditions are value conditions.

Proposition 1 (Lax-Hopf Formula): Let $\psi(\cdot)$ be a concave and continuous Hamiltonian, and let $c(\cdot,\cdot)$ be a value condition. The Barron-Jensen/Frankowska (B-J/F) solution [28], [29] to (9) associated with (10)-(12) is defined by,

$$M_c(t,x)=\inf_{(u,T)\in(\varphi^*\times R_+)}(c(t-T,x+Tu)+T\varphi^*(u)) \tag{13}$$

where φ^* is the Legendre-Fenchel transform of an upper semicontinuous Hamiltonian $\psi(\cdot)$, which is given by,

$$\varphi^*=\sup_{p\in Dom(\psi)}[pu+\psi(p)] \tag{14}$$

By the Lax-Hopf formula, the solutions of equation (9) corresponding to the initial conditions (10) are,

$$M_{M_k}(t,x)=\begin{cases} +\infty, & \text{if } x \le (k-1)X + tw \\ & \text{or } x \ge kX + tv_f \\ -\sum_{i=1}^{k-1}\rho(i)X & \text{if } x \ge (k-1)X + tv_f \\ +\rho(k)(tv_f + (k-1)X - x), & \text{and } x \le kX + tv_f \\ & \text{and } \rho(k) \le \rho_c \\ -\sum_{i=1}^{k-1}\rho(i)X & \text{if } x \le (k-1)X + tv_f \\ +\rho_c(tv_f + (k-1)X - x), & \text{and } x \ge (k-1)X + tw \\ & \text{and } \rho(k) \le \rho_c \\ -\sum_{i=1}^{k-1}\rho(i)X & \text{if } x \le kX + tw \\ +\rho(k)(tw + (k-1)X - x) & \text{and } x \ge (k-1)X + tw \\ -\rho_m tw, & \text{and } \rho(k) \ge \rho_c \\ -\sum_{i=1}^{k}\rho(i)X & \text{if } x \le kX + tv_f \\ +\rho_c(tw + kX - x) & \text{and } x \ge kX + tw \\ -\rho_m tw, & \text{and } \rho(k) \ge \rho_c \end{cases}, \quad (15)$$

the solutions corresponding to the upstream boundary conditions (11) are,

$$M_{\gamma_n}(t,x)=\begin{cases} +\infty, & \text{if } t \le (n-1)T + (x-\xi)/v_f \\ \sum_{i=1}^{n-1} q_{in}(i)T & \text{if } t \ge (n-1)T + (x-\xi)/v_f \\ +q_{in}(n)(t-(x-\xi)/v_f - (n-1)T), & \text{and } t \le nT + (x-\xi)/v_f \\ \sum_{i=1}^{n} q_{in}(i)T & \text{otherwise} \\ +\rho_c v_f(t-(x-\xi)/v_f - nT), & \end{cases}, \quad (16)$$

and the solutions corresponding to the downstream boundary conditions (12) are,

$$M_{\beta_n}(t,x)=\begin{cases} +\infty, & \text{if } t\le (n-1)T+(x-\chi)/w \\ -\sum_{k=1}^{k_{\max}}\rho(k)X+\sum_{i=1}^{n-1}q_{out}(i)T & \\ +q_{out}(n)(t-(x-\chi)/w-(n-1)T) & \text{if } t\ge (n-1)T+(x-\chi)/w \\ -\rho_m(x-\chi), & \text{and } t\le nT+(x-\chi)/w \\ -\sum_{k=1}^{k_{\max}}\rho(k)X+\sum_{i=1}^{n}q_{out}(i)T & \\ +\rho_c v_f(t-(x-\chi)/v_f-nT), & \text{otherwise} \end{cases} . \quad (17)$$

The solutions (15)-(17) are weak solutions and may not be equal to the value condition in its domain. The Lax-Hopf formula leads to the inf-morphism [30] property.

Proposition 2 (Inf-morphism Property): Let the value condition $c(\cdot,\cdot)$ be the minimum of a finite number of lower semicontinuous functions:

$$\forall(t,x)\in[0,t_{\max}]\times[\xi,\chi],\quad c(t,x):=\min_{j\in J}c_j(t,x) \quad (18)$$

The corresponding solution can be decomposed as [31],

$$\forall(t,x)\in[0,t_{\max}]\times[\xi,\chi],\quad M_c(t,x):=\min_{j\in J}M_{c_j}(t,x) \quad (19)$$

where J is the set of the value conditions. Therefore, the Moskowitz solutions (15-17) need to satisfy the compatibility conditions.

Proposition 3 (Compatibility Conditions): The equality $\forall(t,x)\in Dom(c), M_c(t,x)=c(t,x)$ is valid if and only if the inequalities below are satisfied,

$$M_{c_j}(t,x)\ge c_i(t,x),\quad \forall(t,x)\in Dom(c_i),\quad \forall(i,j)\in J^2 \quad (20)$$

The compatibility conditions can be expressed in terms of the Moskowitz functions as follows[21], [23].

$$
\begin{cases}
M_{M_k}(0,pX) \geq M_p(0,pX) & \forall (k,p) \in K^2 \\
M_{M_k}(pT,\chi) \geq \beta_p(pT,\chi) & \forall k \in K, \forall p \in N \\
M_{M_k}(\dfrac{\chi - kX}{v_f},\chi) \geq \beta_p(\dfrac{\chi - kX}{v_f},\chi) & \forall k \in K, \forall p \in N \quad s.t. \dfrac{\chi - kX}{v_f} \in [(p-1)T, pT] \\
M_{M_k}(pT,\xi) \geq \gamma_p(pT,\xi) & \forall k \in K, \forall p \in N \\
M_{M_k}(\dfrac{\xi - (k-1)X}{w},\xi) \geq \gamma_p(\dfrac{\xi - (k-1)X}{w},\xi) & \forall k \in K, \forall p \in N \quad s.t. \dfrac{\xi - (k-1)X}{w} \in [(p-1)T, pT]
\end{cases}, \quad (21)
$$

$$
\begin{cases}
M_{\gamma_n}(pT,\xi) \geq \gamma_p(pT,\xi) & \forall (n,p) \in N^2 \\
M_{\gamma_n}(pT,\chi) \geq \gamma_p(pT,\chi) & \forall (n,p) \in N^2 \\
M_{\gamma_n}(nT + \dfrac{\chi - \xi}{v_f},\chi) \geq \beta_p(nT + \dfrac{\chi - \xi}{v_f},\chi) & \forall (n,p) \in N^2 \quad s.t. nT + \dfrac{\chi - \xi}{v_f} \in [(p-1)T, pT]
\end{cases}, \quad (22)
$$

$$
\begin{cases}
M_{\beta_n}(pT,\xi) \geq \gamma_p(pT,\xi) & \forall (n,p) \in N^2 \\
M_{\beta_n}(pT,\chi) \geq \beta_p(pT,\chi) & \forall (n,p) \in N^2 \\
M_{\beta_n}(nT - \dfrac{\chi - \xi}{w},\xi) \geq \gamma_p(nT - \dfrac{\chi - \xi}{w},\xi) & \forall (n,p) \in N^2 \quad s.t. nT - \dfrac{\chi - \xi}{w} \in [(p-1)T, pT]
\end{cases}. \quad (23)
$$

Above all, the traffic control problem on a single traffic link can be modeled as an LP with constraints (21)-(23), and downstream flows are the decision variables. The inflow matrix q_{in} is predicted from the CTM model through the way illustrated in the previous section, and the initial density matrix ρ is obtained directly from the surveillance system. For the signal control problem at an intersection, one more index indicating the movement should be added to all the variables in (21)-(23), and the constraints for all of the movements shown in Figure 1 should be satisfied.

To model the signal control problem, additional variables and constraints representing signals need to be added. Let $p(r,t)$ equal 1 if the phase r is green at time step t and equal to 0 otherwise; let $r_{\max}$ and $n_{\max}$ be the number of phases and time steps in each cycle, respectively. Then, the following constraints need to be satisfied.

$$
\begin{cases}
\sum_{r\in[1,\,r_{\max}]} p(r,t) \le 1, & \forall t \in [1, n_{\max}] \quad (a) \\
\sum_{t\in[1,\,n_{\max}]} p(r,t) \ge 1, & \forall r \in [1, r_{\max}] \quad (b) \\
p(r,t+1) + \sum_{\substack{r'\in[1,\,r_{\max}] \\ r'\neq r}} p(r',t) \le 1, & \forall r \in [1, r_{\max}], \forall t \in [1, n_{\max}-1] \quad (c) \\
\sum_{r\in[1,\,r_{\max}]} \sum_{i=t}^{t+g_{\min}} p(r,i) \ge g_{\min}, & \forall t \in [1, n_{\max}-g_{\min}] \quad (d) \\
\sum_{r\in[1,\,r_{\max}]} p(r,1) \ge 1, & \quad (e) \\
\sum_{r\in[1,\,r_{\max}]} p(r,n_{\max}) \le 0, & \quad (f) \\
q_{out}(i,t) \le c(i)p(r,t), & \forall i \in I_r, \forall r \in [1, r_{\max}] \quad (g)
\end{cases} \tag{24}
$$

Equation (24.a) indicates that only one phase is green at each time step; (24.b) requires that every phase must be served at least once during each cycle; (24.c) adds lost time, which is equal to one time step in this study, during each phase switch; (24.d) is the constraint for the minimum green time, and $g_{\min}$ is the minimum green time in terms of time steps; (24.e) and (24.f) forces the first time step in each cycle to be green for a phase, and the last time step in each cycle is lost time; these two constraints are used to add lost time at the connection point of two consecutive cycles; the constraint (24.g), where i is the index of movement, $c(i)$ indicates the saturation flow of movement i and I_r is the set of movements served by phase r, and illustrates that the outflow of each movement is controlled by its signal.

We choose to minimize the total travel time in each cycle as the objective function, which is equivalent to minimizing the total delay. The total travel time can be modeled as,

$$
\sum_{i\in I}\sum_{k\in K} \rho(i,k) X n_{\max} + \sum_{i\in I}\sum_{t\in N} q_{in}(i,t) T(n_{\max}-t) - \sum_{i\in I}\sum_{t\in N} q_{out}(i,t) T(n_{\max}-t), \tag{25}
$$

where $\rho(i,k)$ is the initial density of the *k*th segment of the *i*th movement, $q_{in}(i,t)$ and $q_{out}(i,t)$ are the inflow and outflow of the *i*th movement at time step *t*, respectively. The first two terms account for the total time spent at this intersection assuming no vehicles can depart from the intersection, and the third term represents the part overestimated by the first two terms. Because the first two terms are not related to the decision variables, they can be removed, and then, the optimization model can be expressed as,

$$\min_{\mathbf{q_{out}},\mathbf{p}} \quad -\sum_{i\in I}\sum_{t\in N} q_{out}(i,t)T(n_{\max}-t)$$

$$s.t. \quad (21)-(23) \qquad \forall i \in I$$

$$(24) \qquad . \qquad (26)$$

$$q_{out}(i,t) \geq 0 \qquad \forall i \in I, t \in N$$

$$p(r,t) \in \{0,1\} \qquad \forall r \in R, t \in N$$

3.6 Case Study

CORSIM, a microscopic traffic simulator, is employed to implement the proposed adaptive signal control method. CORSIM does not provide traffic densities or vehicle numbers by itself, but we can extract that information with a user-defined interaction module, called Run Time Extension (RTE), written in C++ at the beginning of each cycle. After that, we use the CPLEX_1271 solver in MATLAB to solve the MILP (26) to obtain the optimal solution and give it back to CORSIM through the RTE. The recursive optimization procedure is shown in Figure 3-3.

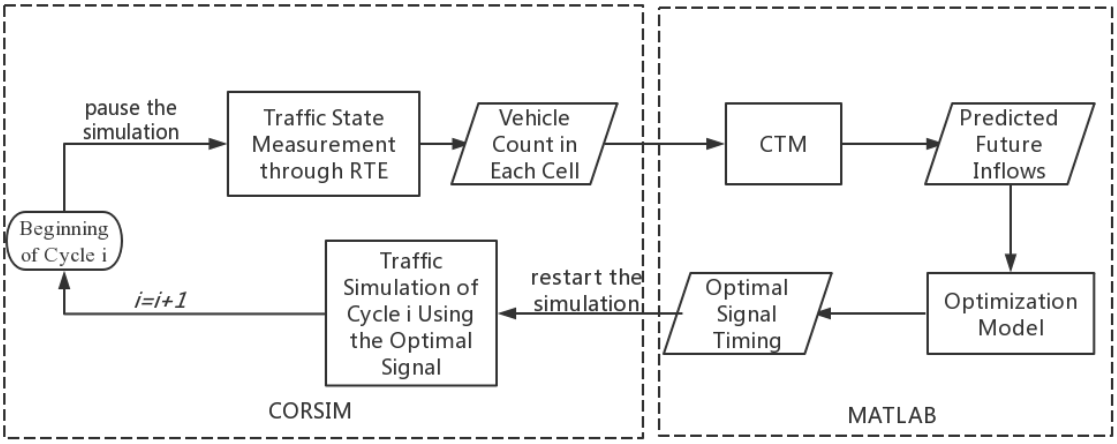

Figure 3-3 Recursive signal control procedure.

Calibration

The tested network is shown in Figure 3-4. Node 1 is the symmetric target intersection, meaning all the incoming links connecting to node 1 have the same geometry and model parameters. The length of the links connected to node 1 is 600 feet, and these links have two lanes: the left lane is for left turn movement only, the right lane is for right turns and through movements. The other links (indicated by thicker arrows) have two unrestricted lanes. For simplicity, the length of those links is set to be 4600 feet so that the traffic volume predictions

for any one cycle do not rely on considering their upstream links. The cycle length is 100 seconds, and the time step is 4 seconds. The free flow speed is 30 mph; the cell length in the upstream links (the thicker ones) is 200 feet; and cell length in the links connecting the target intersection is 100 feet. The simulation time is 1 hour. The turn movement allocations from all links are the same, and the percentages of the left turn, right turn, and through movements are each equal to 1/3. The yellow time in CORSIM is zero because it is difficult to consider them in the optimization model. The all-red time equals one time step (4 s), and the minimum green time is two time steps (8 s).

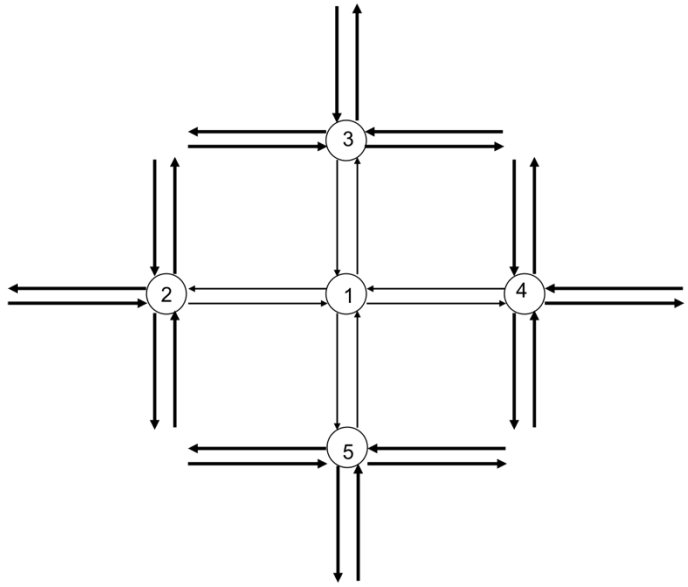

Figure 3-4 Test network.

Saturation flows and jam densities are parameters of both the CTM model and the optimization model, but CORSIM does not output them directly. Therefore, we approximate them under an oversaturation condition. First, high entry inflows are given to the entry nodes to make sure the demand for every movement exceeds its capacity at the target intersection. Then, because the lanes are dedicated for different movements, we use the number of vehicles discharged from each lane divided by its green time ratio as the approximated saturation flow of the corresponding movement. The simulation is run 10 times with different random seeds. The average saturation flows on the left lane (left turn movement) and right lane (through and right turn movement) are 1589 and 1806 vehicles/hour/lane, respectively. The latter value is dependent on the ratio between right turn volume and through volume, which is 1 in this study. In addition, we use the maximum vehicles in each lane (reached when the spillover happens) divided by the queue length to obtain the jam density, and it is equal to 274 vehicles/mile. We assume the parameters of each movement satisfy a triangular fundamental diagram.

To keep matters simple, we give the same entry flows to the links connecting to the same upstream node. For example, the entry flows of the three incoming links of node 2 (excluding link 1-2) are the same, and these links have the same turn movement percentage. In this way, the traffic volume from node 2 to node 1 is equal to the entry flow of each incoming of node 2. The signal timing plans for the upstream nodes have a cycle length of 100 s, and

they are shown in Table 3-1. The index of the movements is the same as Figure 3-1. These splits are obtained through the critical lane flow ratio method [32]. There is no offset on any of these signals.

Table 3-1 Signal timing plan for upstream nodes

Phase number	1	2	3	4
Movements (nodes 3 and 5)	*1 & 2*	*3 & 4*	*5 & 6*	*7 & 8*
Green Time (s)	12	28	12	28
All Red Time (s)	4	4	4	4
Movements (nodes 2 and 4)	*7 & 8*	*5 & 6*	*3 & 4*	*1 & 2*
Green Time (s)	28	12	28	12
All Red Time (s)	4	4	4	4

3.7 Results

Webster [33] proposed a model to determine the green splits,

$$g_r = \frac{\max\left\{\frac{v(i)}{c(i)} : i \in I_r\right\}}{\sum_{r\in[1,r_{\max}]} \max\left\{\frac{v(i)}{c(i)} : i \in I_r\right\}}\left(C-L\right) \tag{27}$$

where C is the cycle length, L is the total lost time in one cycle, $v(i)$ is the lane volume of movement i and $c(i)$ is the saturation flow per lane of movement i.

$$\max\left\{\frac{v(i)}{c(i)} : i \in I_r\right\}$$

is called the critical lane flow ratio of phase r. The interpretation of this method is that the phases should be split proportionally to the critical lane flow ratio. Another method was proposed by the Highway Capacity Manual [32] to ensure all stages have the same critical v/c ratio. Both methods lead to the same solutions. In this section, the total delay per vehicle resulting from our method is compared with the methods based on critical lane flow ratios.

We use the overall critical volume-to-capacity ratio defined below to represent the degree of congestion,

$$\lambda = \frac{C}{G}\sum_{r\in[1,r_{\max}]} \max\left\{\frac{v(i)}{c(i)} : i \in I_r\right\} \tag{28}$$

where G is the total green time in one cycle and equal to the cycle length minus the total red time. All the scenarios in this section are undersaturated and no spillback happens during the simulations.

First, we consider the case with balanced inflows, which means the entry flows to each entry node are the same. To remove the influence of the randomness, every single scenario is run 10 times. Table 3-2 shows the one-tailed paired t-test of the total delay per vehicle between two methods. With the decrease of the overall critical *v/c* ratio, the reduction of the delay increases; the effect of the proposed model is significant when the overall critical ratio is below 83.4%. The following restrictions in our model could be the main factors that limit the model's performance when the traffic volume approaches saturation: the proposed model does not consider the start-up delay which exists in the CORSIM simulation; in addition, the optimal phase splits must be multiples of the time step rather than arbitrary integer numbers.

Table 3-2 One-tailed paired t-test of the total delay per vehicle (s) under balanced traffic conditions.

Run index	Entry flow (vph)									
	200		400		500		600		650	
	Proposed method	HCM method	Proposed method	HCM method	Proposed method	HCM method	Proposed method	HCM method	Proposed method	HCM method
1	18.9	23.5	24.4	28.4	28.0	31.2	35.4	38.1	40.1	47.1
2	18.4	25.0	23.4	28.0	28.3	30.0	31.8	33.6	36.6	38.4
3	19.0	25.2	24.8	28.4	27.6	31.9	34.6	37.2	40.7	42.8
4	18.8	28.3	24.1	30.4	28.8	32.4	35.9	36.0	40.2	40.4
5	19.4	24.3	24.3	28.0	27.8	30.5	35.5	36.2	38.0	37.9
6	20.6	25.7	25.4	29.6	30.2	32.9	34.4	35.1	44.1	39.7
7	18.7	25.3	23.0	28.6	27.2	30.7	35.4	35.0	40.1	39.6
8	19.4	24.8	23.9	29.5	29.4	33.1	35.1	37.2	45.8	47.4
9	18.4	24.2	23.4	28.0	26.4	29.4	33.1	33.7	36.7	39.3
10	18.4	24.3	25.0	28.9	28.8	31.9	33.4	36.0	41.0	41.4
Mean	19.0	25.0	24.2	28.8	28.3	31.4	34.5	35.8	40.3	41.4
Reduced (%)	24.2		16.1		10.0		3.8		2.6	
p-value	1.2e-7		3.7e-8		8.3e-8		0.002		0.138	
λ (%)	27.8		55.6		69.5		83.4		90.3	

Table 3-3 One-tailed paired t-test of the total delay per vehicle (s) under partially unbalanced traffic conditions.

	Entry flow (vph)											
	N-S 100 E-W 400		N-S 200 E-W 300		N-S 200 E-W 500		N-S 300 E-W 400		N-S 400 E-W 600		N-S 450 E-W 500	
Run index	Proposed method	HCM method	Proposed method	HCM method	Proposed method	HCM method	Proposed method	HCM method	Proposed method	HCM method	Proposed method	HCM method
1	16.9	24.7	19.0	24.6	20.3	26.5	21.4	26.5	28.6	30.9	26.8	30.6
2	17.1	25.8	20.2	27.2	20.5	28.2	21.7	27.0	26.4	29.2	27.9	29.5
3	17.6	25.4	20.1	26.7	21.2	28.3	21.8	27.5	27.9	31.3	28.3	31.4
4	19.2	28.2	20.7	29.8	22.0	31.0	22.1	30.4	28.9	32.5	29.2	32.8
5	17.4	25.4	20.3	25.9	20.8	27.7	22.4	26.4	28.3	30.1	28.4	29.7
6	17.3	28.5	20.3	28.3	22.4	30.7	22.9	28.4	29.8	31.7	30.2	31.3
7	17.6	25.9	19.2	27.3	20.7	28.2	22.3	27.5	27.1	30.2	28.1	29.7
8	17.9	26.2	19.0	26.5	22.4	28.8	22.1	28.0	32.4	33.0	27.9	32.7
9	17.3	25.3	18.0	24.7	20.5	27.4	22.5	26.8	26.9	30.1	27.2	29.0
10	19.3	25.9	19.1	26.0	22.1	28.6	22.9	27.3	29.8	31.1	28.5	31.9
Mean	17.8	26.1	19.6	26.7	21.3	28.5	22.2	27.6	28.6	31.0	28.3	30.8
Reduced (%)	32.0		26.7		25.4		19.5		7.8		8.4	
p-value	1.6e-9		3.9e-9		4.6e-10		9.7e-8		1.38e-5		6.05e-5	
λ (%)	34.7				48.6				70.0			

Figure 3-5 and Figure 3-6 show the Moskowitz solutions of the 3rd phase resulting from the proposed method in two consecutive cycles under entry flows of 400 vph and 600 vph, respectively. The color denotes the density, and the black lines represent the vehicle trajectories. The yellow part at the downstream boundary indicates the congestion caused by the red signal, and the blue part that follows represents the queues dissipating during the green time. Figure 3-5 and Figure 3-6 show that the number of switchovers under low traffic volumes is more than at high traffic volumes. Under low traffic volumes, more switchovers increase the throughput to reduce the total traffic delay. On the other hand, because more switchovers lead to more lost time and increase the traffic delay when the traffic volume is high, the signal is mainly controlled by the sequence and phase splits. Although a phase may be served more than once in a single cycle as shown in Figure 3-6, the average number of switchovers is significantly less than in the cases with low traffic volumes.

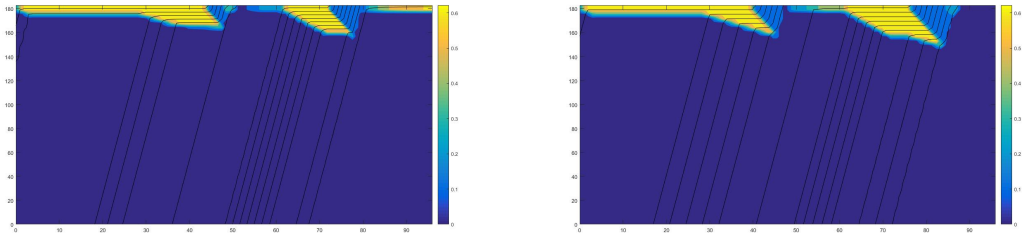

(a). The first cycle (b). The second cycle

Figure 3-5 Moskowitz solution with entry flows of 400 vph.

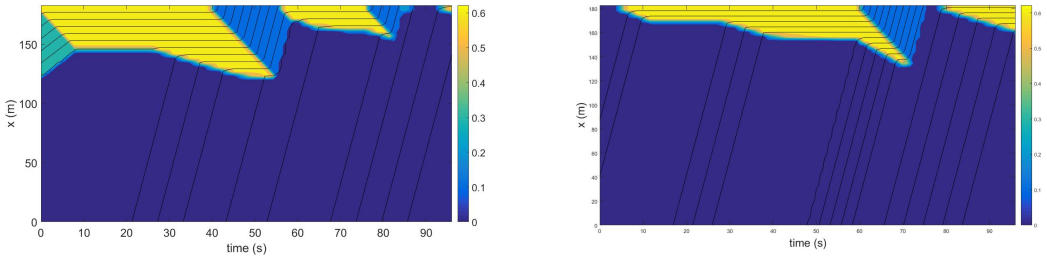

(a). The first cycle (b). The second cycle

Figure 3-6 Moskowitz solution with entry flows of 600 vph.

Table 3-3 shows the result under partially unbalanced traffic volumes. In this table, nodes 3 and 5 (2 and 4) have the same entry flows, and they differ from nodes 2 and 4 (3 and 5). N, S, E, W denote the traffic volumes from nodes 3, 5, 4 and 2, respectively. As in Table 3-2, the delay reduction increases with the decrease of the critical *v/c* ratio. For the scenarios with the same critical *v/c* ratio, the reduction is larger when the difference between the entry flows from different directions is larger

In order to investigate the influence of the traffic volume difference between the movements in the same phase, the completely unbalanced scenarios are also studied. In these scenarios, the traffic volumes from all four approaches are different. Comparisons of total delay

per vehicle are shown in Table 3-4. Table 3-2 through Table 3-4 show the proposed method can reduce the travel delay effectively under various traffic conditions. Because this optimization model takes all of the movements into account while the HCM method only considers the movements with the critical lane flow, the travel delay reduction percentage for the unbalanced case is more than the balanced case with the same overall critical volume-to-capacity ratio.

Table 3-4 One-tailed paired t-test of the total delay per vehicle (s) under completely unbalanced traffic conditions.

	Entry flow (vph)			
	N 400 S 200 E 300 W 500		N 300 S 200 E 400 W 500	
Run index	Proposed method	HCM method	Proposed method	HCM method
1	24.1	27.5	22.1	26.3
2	23.1	28.0	22.0	27.4
3	24.2	28.4	22.1	27.8
4	23.8	30.8	22.3	30.6
5	23.0	27.9	21.4	27.1
6	24.6	30.9	22.9	29.9
7	23.7	28.8	21.6	27.5
8	22.6	29.0	21.3	28.7
9	22.5	27.0	21.5	26.7
10	23.4	28.6	22.1	27.9
Mean	23.5	28.7	21.9	28.0
Reduced (%)	18.1		21.7	
p-value	5.0e-8		3.0e-8	
λ (%)	62.5		55.6	

3.8 Summary

The adaptive signal control method including the traffic volume prediction model and the signal optimization model is presented in this chapter. The effectiveness of the proposed framework is compared to the critical lane flow method through microscopic traffic simulations in CORSIM. It shows the proposed model can reduce the traffic delay significantly under a wide range of degree of saturation.

Chapter 4. Summary and Conclusions

4.1 Introduction

This chapter summarizes the findings and conclusions from this work as well as provides suggestions for future work.

4.2 Summary and Conclusions

We propose an adaptive signal control algorithm for an isolated intersection under undersaturated traffic conditions. This methodology employs a movement-based CTM model to predict the traffic volume according to the current upstream traffic states measured from the surveillance system. The signal control is modeled as a MILP based on the analytical solution of the LWR model. The phase sequence, phase splits, and number of switchovers can be optimized at the same time. Compared to the Highway Capacity Manual's critical lane flow approach, our method can reduce the total delay per vehicle effectively under various traffic conditions.

4.3 Directions for Future Research

In the future, the proposed method can be improved in the following ways:

1. The start-up delay is not considered in the CTM model and optimization model. By taking the start-up delay into account, both the accuracy and the effectiveness of the model can be improved.
2. The time to solve the MILP is not quick enough to make this method practical. Under the premise of ensuring the efficiency, one might develop an approximation method to reduce the computation time.
3. The proposed model is working for an isolated intersection with undersaturated conditions. It would be promising to develop an optimization model for an arterial street or a network level.
4. Use the link transmission model (LTM) instead of CTM if the traffic volumes of more upstream nodes need to be predicted.

References

[1] P. B. Hunt, D. I. Robertson, and R. D. Bretherton, "The SCOOT on-line traffic signal optimisation technique," *Traffic Eng. Control*, vol. 23, no. 4, 1982.

[2] P. Lowrie, "Scats, sydney co-ordinated adaptive traffic system: A traffic responsive method of controlling urban traffic," 1990.

[3] A. Miller, "A Computer Control System for Traffic Networks.," in *Second International Symposium on Theory of Traffic Flow*, 1963.

[4] K.-L. Bång and L.-E. Nilsson, "Optimal Control of Isolated Traffic Signals," *IFAC Proc. Vol.*, vol. 9, no. 4, pp. 173–184, Aug. 1976.

[5] N. H. Gartner, "OPAC: A demand-responsive strategy for traffic signal control," *Transp. Res. Rec.*, no. 906, pp. 75–81, 1983.

[6] K. L. Head, "Event-based short-term traffic flow prediction model," *Transp. Res. Rec.*, no. 1510, pp. 45–52, 1995.

[7] S. Sen and K. L. Head, "Controlled Optimization of Phases at an Intersection," *Transp. Sci.*, vol. 31, no. 1, pp. 5–17, 1997.

[8] P. Mirchandani, "A real-time traffic signal control system: architecture, algorithms, and analysis," *Transportation Res. Part C Emerg. Technol.*, vol. 9, no. 6, pp. 415–432, 2001.

[9] C. Cai, C. K. Wong, and B. G. Heydecker, "Adaptive traffic signal control using approximate dynamic programming," *Transp. Res. Part C Emerg. Technol.*, vol. 17, no. 5, pp. 456–474, 2009.

[10] X. Zheng, W. Recker, and L. Chu, "Optimization of control parameters for adaptive traffic-actuated signal control," *J. Intell. Transp. Syst. Technol. Planning, Oper.*, vol. 14, no. 2, pp. 95–108, 2010.

[11] X. Zheng and W. Recker, "An adaptive control algorithm for traffic-actuated signalized networks," *Transp. Res. Part C Emerg. Technol.*, vol. 30, pp. 93–115, 2013.

[12] G. F. Newell, "The rolling horizon scheme of traffic signal control," *Transp. Res. Part A Policy Pract.*, vol. 32, no. 1, pp. 39–44, 1998.

[13] P. B. Mirchandani and N. Zou, "Queuing Models for Analysis of Traffic Adaptive Signal Control," *IEEE Trans. Intell. Transp. Syst.*, vol. 8, no. 1, pp. 50–59, Mar. 2007.

[14] K. Aboudolas, M. Papageorgiou, A. Kouvelas, and E. Kosmatopoulos, "A rolling-horizon quadratic-programming approach to the signal control problem in large-scale congested urban road networks," *Transp. Res. Part C Emerg. Technol.*, vol. 18, no. 5, pp. 680–694, 2010.

[15] E. Christofa, K. Ampountolas, and A. Skabardonis, "Arterial traffic signal optimization: A person-based approach," *Transp. Res. Part C Emerg. Technol.*, vol. 66, pp. 27–47, 2016.

[16] H. K. Lo, "A reliability framework for traffic signal control," *IEEE Trans. Intell. Transp. Syst.*, vol. 7, no. 2, pp. 250–260, 2006.

[17] L. Li, W. Huang, and H. K. Lo, "Adaptive coordinated traffic control for stochastic demand," *Transp. Res. Part C Emerg. Technol.*, vol. 88, no. January, pp. 31–51, 2018.

[18] W. Ma, K. An, and H. K. Lo, "Multi-stage stochastic program to optimize signal timings under coordinated adaptive control," *Transp. Res. Part C Emerg. Technol.*, vol. 72, pp. 342–359, 2016.

[19] C. F. Daganzo, "The cell transmission model: A dynamic representation of highway traffic consistent with the hydrodynamic theory," *Transp. Res. Part B Methodol.*, vol. 28, no. 4, pp. 269–287, Aug. 1994.

[20] C. F. Daganzo, “The cell transmission model, part II: Network traffic,” *Transp. Res. Part B Methodol.*, vol. 29, no. 2, pp. 79–93, Apr. 1995.
[21] E. S. Canepa and C. G. Claudel, “Exact solutions to traffic density estimation problems involving the Lighthill-Whitham-Richards traffic flow model using mixed integer programming,” in *Intelligent Transportation Systems (ITSC), 2012 15th International IEEE Conference on*, 2012, pp. 832–839.
[22] C. G. Claudel and A. M. Bayen, “Convex formulations of data assimilation problems for a class of Hamilton--Jacobi equations,” *SIAM J. Control Optim.*, vol. 49, no. 2, pp. 383–402, 2011.
[23] E. S. Canepa and C. G. Claudel, “Spoofing cyber attack detection in probe-based traffic monitoring systems using mixed integer linear programming,” in *Computing, Networking and Communications (ICNC), 2013 International Conference on*, 2013, pp. 327–333.
[24] E. S. Canepa and C. G. Claudel, “Networked traffic state estimation involving mixed fixed-mobile sensor data using Hamilton-Jacobi equations,” *Transp. Res. Part B Methodol.*, vol. 0, pp. 1–24, 2016.
[25] M. J. Lighthill and G. B. Whitham, “On kinematic waves. II. A theory of traffic flow on long crowded roads,” in *Proceedings of the Royal Society of London A: Mathematical, Physical and Engineering Sciences*, 1955, vol. 229, no. 1178, pp. 317–345.
[26] K. Moskowitz, “Discussion of `freeway level of service as influenced by volume and capacity characteristics’ by DR Drew and CJ Keese,” *Highw. Res. Rec.*, vol. 99, pp. 43–44, 1965.
[27] C. D.-T. R. P. B. Methodological and undefined 2005, “A variational formulation of kinematic waves: basic theory and complex boundary conditions,” *Elsevier*.
[28] E. N. Barron and R. Jensen, “Semicontinuous Viscosity Solutions For Hamilton–Jacobi Equations With Convex Hamiltonians,” *Commun. Partial Differ. Equations*, vol. 15, no. 12, pp. 293–309, Jan. 1990.
[29] H. Frankowska, “Lower Semicontinuous Solutions of Hamilton–Jacobi–Bellman Equations,” *SIAM J. Control Optim.*, vol. 31, no. 1, pp. 257–272, Jan. 1993.
[30] J.-P. Aubin, A. M. Bayen, and P. Saint-Pierre, “Dirichlet problems for some Hamilton--Jacobi equations with inequality constraints,” *SIAM J. Control Optim.*, vol. 47, no. 5, pp. 2348–2380, 2008.
[31] C. G. Claudel and A. M. Bayen, “Lax–Hopf Based Incorporation of Internal Boundary Conditions Into Hamilton–Jacobi Equation. Part I: Theory,” *IEEE Trans. Automat. Contr.*, vol. 55, no. 5, pp. 1142–1157, May 2010.
[32] TRB, “Highway Capacity Manual,” in *Special Report 209, third edition*, 1994.
[33] F. Webster, “Traffic signal settings, road research technical paper no. 39,” *Road Res. Lab.*, 1958.